Angularly resolved rotationally inelastic scattering of Na_2-Ne: Comparison between experiment and theory

P. L. Jones, U. Hefter, A. Mattheus, J. Witt, and K. Bergmann
Fachbereich Physik der Universität, P. O. Box 3049, D-6750 Kaiserslautern, West Germany

W. Müller and W. Meyer
Fachbereich Chemie der Universität, P. O. Box 3049, D-6750 Kaiserslautern, West Germany

R. Schinke
Max-Planck-Institut für Strömungsforschung, Böttingerstrasse 6-8, D-3400 Göttingen, West Germany
(Received 18 March 1982)

The results of a systematic experimental and theoretical investigation of the differential cross sections for vibronically elastic, rotationally inelastic scattering of Na_2 from Ne at a center-of-mass collision energy of 190 meV are presented. The experimental cross sections cover the range of rotational transitions $\Delta j=2$ to $\Delta j=20$ for a variety of initial rotational levels including the initially rotationless level $j_i=0$. The data document clearly the major features of rotationally inelastic scattering for collisional systems with steeply repulsive, strongly anisotropic interaction potentials and many energetically open channels, such as main and supernumerary rotational rainbows. The experimental curves are transformed into the center-of-mass reference frame using a constrained minimalization procedure. They are compared with those calculated within the infinite-order sudden approximation from an *ab initio* potential surface which includes configuration interaction. The results show that the theoretical curves faithfully reproduce both the form and relative magnitudes of the experimental cross sections. An analysis of the sensitivity of the agreement between theory and experiment as the potential is systematically varied indicates that the experimental data place a limit of about $\pm 5\%$ on the accuracy of the calculated anisotropy. The steepness of the *ab initio* potential could be varied by -10% or $+25\%$ and still lead to an acceptable agreement of calculated and experimental cross sections. The variation of the cross section at the rainbow maximum with Δj and j_i is shown to be an unreliable test of the accuracy of the potential-energy surface unless a large range of Δj is studied. Finally, it is found that all data from a large set of calculated but also partially experimentally verified integral cross sections fall near a single curve when plotted as reduced cross sections versus transferred energy ΔE, according to a power-gap fitting law. Different power exponents are, however, needed to describe the variation of the cross sections with ΔE for very small and larger energy transfer.

I. INTRODUCTION

Central to the understanding of chemical processes and responsible for the maintenance of equilibrium, the transfer of energy and momentum is a recurring theme at all levels of physics. For the simple case of translational to rotational energy and momentum transfer in atom-diatom collisions, experiments have only recently elucidated the main features of the collision dynamics. Following the pioneering work of the early sixties on collisional energy transfer in molecular beams involving TlF (Ref. 1) and D_2 (Ref. 2) rotationally inelastic collisions were studied mainly through the measurement of rate constants for transitions between well-defined quantum states of molecules undergoing collisions (see for example Ref. 3–7). These measurements were carried out for molecules in their electronically excited states[3,7] as well as their ground states.[4–6] However the inherent averaging in the measured rate constants made it difficult to draw detailed conclusions regarding the collision dynamics or the form of the interaction potential from the data.

Significant progress in the understanding of the detailed dynamics of rotational energy and momentum transfer was made with the successful completion of beam experiments with state-selected molecules. Because of the relative ease of ion detection, ion-molecule collisions were the first to be

studied on a state-to-state level in beams.[8] Similar experiments with neutral particles were first completed for the Ne-HD collision system,[9] followed by other experiments involving hydrogenic molecules.[10] Application of laser methods opened for study molecules such as Na_2 which in contrast to hydrogenic molecules have closely spaced rotational levels.[11–17] At the same time Beck *et al.*[18] resolved structure in the angularly resolved energy-loss spectrum of K atoms colliding with N_2 and CO. Very recently refinements of the time-of-flight technique have permitted the resolution of single rotational transitions in collisions of He with N_2, CO, and CH_4.[19] A review of recent progress in this field is given in Refs. 20 and 21.

To date two characteristically different types of neutral collision systems, both involving predominantly repulsive interactions, have been studied. The systems Ne-D_2 and He-CO represent the weak-coupling case where diffraction oscillations, well known from the study of elastic atom-atom scattering,[22] are the dominant feature of both the rotationally elastic and inelastic differential cross sections. For the Ne-D_2 collision pair a direct inversion of the experimental data to obtain the potential-energy surface has been performed.[23] The collision systems K-CO (Ref. 18) or He-Na_2 (Ref. 13) belong to the strong-coupling case where rotational rainbows, a new kind of systematic structure, prevail. Referring to a semiclassical picture, they stem from the interference of trajectories with different initial parameters leading to the same angular momentum transfer Δj *and* the same scattering angle. This phenomenon has been analyzed by various authors using classical mechanics[24–27] as well as approximate quantum treatments.[28–33] An overview article has recently been published by Schinke and Bowman.[34] For the strong-coupling case a direct inversion of scattering data has been carried out only in a model calculation.[35] The results of that study demonstrated the need for scattering data of very high quality if an inversion procedure is to be successfully applied for strong collision pairs.

In the present paper we report the results of a systematic experimental and theoretical investigation of rotationally inelastic scattering of Na_2 from Ne. The experimentally accessible range of rotational transitions is not yet large enough to make an inversion of the data feasible. The data set is large enough, however, to apply a complementary approach. Here we compare the measured differential cross sections with those calculated within the infinite-order sudden (IOS) approximation using an *ab initio* potential surface. Besides elucidating the major features of rotationally inelastic scattering for the strong-coupling case of repulsive interactions, the data provide a test of the applicability of the dynamical approximations and the accuracy of the *ab initio* interaction potential.

The paper is divided into eight parts. In Sec. II the experimental details pertaining to the measurement of the differential cross sections are presented along with three representative experimental differential cross sections in the laboratory frame of reference. All other experimental cross sections will be presented in the center-of-mass reference frame. In Sec. III the method of calculation and the resulting potential-energy surface for the Na_2-Ne collision pair are described. A short discussion of the rotational rainbow structure with particular emphasis on the Na_2-Ne system and the relevant details of the scattering calculations are outlined in Sec. IV, while in Sec. V the transformation of the experimental cross sections is described. Section VI contains the comparison of calculated and measured cross sections. In Sec. VII we examine the extent to which the *ab initio* potential-energy surface is verified by the presently available experimental data. The results are finally summarized in Sec. VIII.

II. EXPERIMENTAL

The technique of measuring rotationally inelastic state-to-state differential cross sections using a combination of optical pumping to select the initial state and laser-induced fluorescence to detect the final state has been described in detail previously.[13] Figure 1 shows schematically the arrangement of the crossed-beams experiment. A supersonic Na/Na_2 beam having a mean velocity of $v=1415\pm5$ m/sec and a velocity spread $\Delta v/v=0.18$ is produced by expanding pure sodium at a vapor pressure of approximately 50 Torr (927 K) through a 0.5-mm orifice. After collimation with rectangular slits (1×3 mm) to a full-angle divergence of 1.5°, the beam travels into the collision chamber and intersects a supersonic neon beam at 90° approximately 100 mm from the source. The neon beam has a mean velocity of $v=770\pm15$ m/sec, a velocity spread $\Delta v/v=0.07$, and a full-angle divergence of approximately 3.5°. From the measured beam intensity profiles the collision volume is roughly estimated to be of the order of 8 mm^3. The collision energy is 190 meV.[36] The rotational-level population of sodium dimers is non-thermal, but can be described approximately by a rotational temperature of the order of 40 K.[13,37]

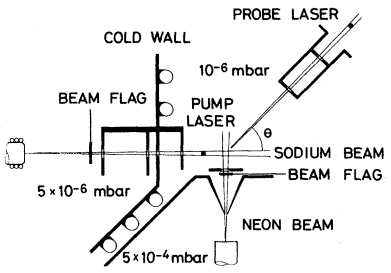

FIG. 1. Experimental apparatus drawn approximately to scale. A liquid-nitrogen-cooled wall separates the sodium oven chamber and the scattering chamber. The collimating slits are cooled but can be heated in order to free clogged slits. The probe and pump laser beams are perpendicular to the plane of the molecular beam.

Sodium dimers in a definite final rotational state j_f of the ground vibrational and electronic state are detected at the variable scattering angle θ after single collisions with neon atoms using laser-induced fluorescence. The angle θ is measured to within $\pm 0.1°$ with an angle decoding system. The zero of the angle scale is determined for each experimental run by measuring the primary beam (Na/Na_2) profile. The detection system[38,39] consists of a single-mode dye laser (CR 599-21) operating at frequencies corresponding to Na_2 ($A\,^1\Sigma_u^+ v' = 17 \leftarrow X\,^1\Sigma_g^+ v'' = 0$) transitions.[40] The laser beam is brought to the detector through the 50-μm core of a single optical fiber and has a residual polarization of less than 5% upon exciting the fiber. An estimated 20% of the induced fluorescence is collected and imaged onto a fiber bundle. This fiber bundle transfers the fluorescence to a cooled RCA 31034 A photomultiplier. The overall detection efficiency is estimated to be 1%.[38,39]

The intensity of the measured fluorescence is proportional to the population-weighted sum of all collisional processes that leave a sodium dimer in the state j_f and at the angle θ. Thus one writes for the fluorescence signal at the angle θ,

$$I(j_f \mid \theta) = D \sum_i n_i \sigma(j_f \leftarrow j_i \mid \theta) , \tag{1}$$

where D is the proportionality factor including detector efficiency and geometry, beam fluxes, etc., n_i is the population of the ith state, and $\sigma(j_f \leftarrow j_i \mid \theta)$ is the differential cross section for making the transition $j_i \rightarrow j_f$.

Since the contribution to the measured fluorescence intensity $I(j_f \mid \theta)$ from a single transition $j_i \rightarrow j_f$ depends linearly on the population, one can isolate a single state-to-state differential cross section by using a single-mode dye laser to deplete the population of the initial level j_i upstream of the collision center. When the pump laser is intensity modulated, a modulation proportional to the j_i-to-j_f differential cross section is observed,

$$\Delta I(j_f \leftarrow j_i \mid \theta) = D P n_i \sigma(j_f \leftarrow j_i \mid \theta) . \tag{2}$$

The factor P is the fractional depletion of the population in level i which occurs with the pump laser on. For this experiment P is greater than 0.98. In deriving the above expression it is assumed that the contributions to $\Delta I(j_f \leftarrow j_i \mid \theta)$ from higher vibrational states over which the population of j_i has been distributed are small. For the present system this approximation is expected to hold.[13]

The state-to-state differential cross sections are measured by scanning the detector through the desired laboratory angular range in steps of $\Delta\theta = 0.5°$. The minimum measurable laboratory angle is 3.5°, the angle at which the detector begins to see the wings of the primary beam profile. The maximum angle is roughly 40° and is imposed by the kinematics of the Na_2-Ne collision system with the aforementioned experimental parameters. At each angle two signal and two background channels are measured with a 2-sec integration time per channel. The difference signal $\Delta I(j_f \leftarrow j_i \mid \theta)$ can then be calculated. After a complete scan of the angular range the laser frequencies are checked, adjusted if necessary, and the scan repeated. The final cross sections are the sum of 10 to 30 such scans. During the experiment all signal channels and control functions are monitored with a Dietz Minical 621 computer system.[41]

Figure 2 shows three measured differential cross sections versus laboratory scattering angle. The intensity units are arbitrary due to the lack of ade-

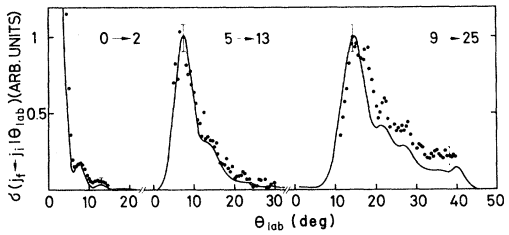

FIG. 2. Three experimentally measured differential cross sections in the laboratory reference frame that illustrate the range and quality of the original data. Solid lines are IOS cross sections transformed to the laboratory frame. Experimental and calculated curves are normalized to unity at the rainbow maximum, except for the $j_i = 0$ to $j_f = 2$ curve, where an arbitrary scale for more convenient presentation of the supernumerary rainbows is chosen.

quate information concerning the value of the proportionality constant D in Eq. (2). The error in the intensity is taken to be $\sqrt{2N}$, where N is the largest of the four measured count rates. The error in the angle based upon an analysis of the detector geometry and Na_2-Ne kinematics is less than 2° between the angle 0° and 30°.[14,42] The three cross sections illustrate the range in Δj and the quality of the experimentally measured cross sections. The solid line is a theoretically calculated cross section which will be discussed in detail in Sec. VI. The set of experimental results for the Na_2-Ne collision system consists of 14 cross sections from the present study plus seven from a previous study[14,15] and cover the range of Δj from 2 to 24 with j_i from 0 to 20.

III. POTENTIAL-ENERGY SURFACE

A. Method of calculation

The potential-energy surface of the Na_2-Ne collision system has been calculated using *ab initio* techniques which employ sufficiently large basis sets and give reliable interaction energies. The atomic basis sets have been optimized for a Na_2-Ne distance of $R=3.5$ Å in C_{2v} and $C_{\infty v}$ symmetry which is near the classical turning point for both orientations at a collision energy of 190 meV. For each sodium atom an 11*s*, 5*p* set of Gaussian-type functions has been employed. For neon a basis set of 8*s*, 4*p*, and 2*d* functions has been used. The exponents of the two complete sets of *d*-type functions have been chosen to provide an optimal description of electron correlation and polarizability in the neon atom. This is necessary for a proper description of the dispersion attraction between the two interacting subsystems.

Electron correlation effects have been considered for all *L*-shell orbitals of neon together with the bond orbital of the sodium molecule using the method of self-consistent electron pairs (SCEP).[43] This iterative procedure is completely equivalent to a configuration-interaction (CI) calculation in the space of *all* singly and doubly substituted configurations constructed from the Hartree-Fock ground-state Slater determinant. Electron correlation effects have been found to be very important even in the repulsive part of the potential which is dominated by the Hartree-Fock repulsion between the two subsystems. Moreover, the relative importance of the correlation energy contributions to the interaction energy depends critically on the orientation between the two subsystems. This strongly affects the anisotropy of the potential, the most important feature for rotational excitation. For example, electron correlation effects increase the anisotropy by as much as 20% at an energy of 190 meV.[44]

The accuracy of the *ab initio* potential has been estimated from calculations with larger basis sets. The error in the calculated interaction energies in the repulsive wall of the potential around 100 meV is expected to be on the order of 5% which corresponds to a variation in the radial distance R of less than 0.03 Å. As will be discussed in Sec. VII this estimate of the accuracy for the *ab initio* potential is consistent with the experimental results. A large part of the remaining error is due to the neglect of intershell correlation in Na_2, an effect which contracts the valence shell of Na_2 and therefore is expected to reduce the repulsion slightly. It should also be pointed out that the calculations have not been designed to reproduce the long-range tail of the potential quantitatively. Details of the potential-energy calculation are discussed in Ref. 44.

B. Interaction potential

The interaction potential $V(R,\gamma)$ has been calculated at 47 points covering the range in intersubsystem distance R of 2 to 10 Å and four different orientation angles $\gamma=0°$, 30°, 60°, and 90° of the molecular axis relative to the incoming particle. The calculated potential-energy points are given in Table II of Ref. 44. The equilibrium internuclear separation $r_e=3.0787$ Å of the sodium molecule[45] was used as the Na-Na distance in the calculations. Previous theoretical studies of Na_2-He inelastic scattering have demonstrated that the inclusion of vibrational excitation of the sodium molecule only slightly affects the rotational excitation cross sections.[46] Similar results are expected to be true for Na_2-Ne, therefore the calculations are confined to the vibrationally elastic case.

To give a compact analytical representation of the global interaction potential an expression similar to that successfully applied for the Na_2-He system[47] has been developed. The expression for Na_2-He has been extended in the description of the attractive part of the potential-energy surface to account for the larger intersubsystem attraction in the Na_2-Ne system. In the present case the expression becomes

$$V_{\mathrm{CI}}(R,\gamma)=\sum_{k=1}^{2} a_1\exp(-a_2R_k)$$
$$+\sum_{l=1}^{3} b_l\exp(-c_lR-d_lR^2)$$
$$\times P_{2(l-1)}(\cos\gamma)$$
$$+e(R-f)^{-6}G^2[g(R-h)]\ . \qquad (3)$$

The parameters $x=e$, f, g, and h include angular dependencies according to $x=x_1+x_2P_2(\cos\gamma)$. The P_λ $(\cos\gamma)$ are Legendre polynomials and

$$G(y)=1-(1+y+1/2y^2)\exp(-y)$$

is a cutoff function. The first term of the above equation is designed to reproduce the higher-order anisotropies which occur at short radial distances due to the interaction of Ne with the Na inner cores. The variables R_1 and R_2 are the two Ne-Na internuclear separations. The second term of the equation describes the repulsive interaction between the neon atom and the bond orbital of Na_2. The last term parametrizes the dispersion attraction. The 19 parameters a_1 through h_2 have been optimized using a least-squares-fit procedure and are given in Table I. Equation (3) reproduces the *ab initio* energies with a mean relative accuracy of 1.9%. The agreement is better than 5% for all values. Note that this fit is valid within the (R,γ) range covered by the *ab initio* calculations and should not be used for shorter radial distances.

The interaction potential $V_{\mathrm{CI}}(R,\gamma)$ is plotted in Fig. 3(a) for $\gamma=0°$ and 90° and is given in polar coordinates in Fig. 3(b) as curves of constant potential. The outermost contour corresponds to the van der Waals minimum at large radial distances. The dotted line is the zero-energy contour. Starting with $E=2$ meV the solid lines represent contours with a factor of 10 increase in energy. They may be regarded as the curves of classical turning points for backward scattering with the respective energies. Qualitatively the potential-energy surface (PES) may be divided into three different regimes. First at large radial distances R the interaction is governed by the dispersion attraction which is due to the dynamical polarizability of the interacting charge distributions. With the approach of the two subsystems the repulsive exchange interaction between the sodium bonding electrons and those in the neon atom increases and finally dominates over the dispersion attraction. The result is a very shallow van der Waals minimum with a calculated well depth ϵ of roughly 0.3 meV. From calculations on Ne-H_2 with similar basis sets and comparison with experimental data[23] the true well depth is estimated to be 0.4—0.5 meV, depending on the orientation. The second regime, at intermediate distances $3.5\lesssim R\lesssim 6$ Å, is characterized by the repulsive interaction of the neon atom with the bond orbital of

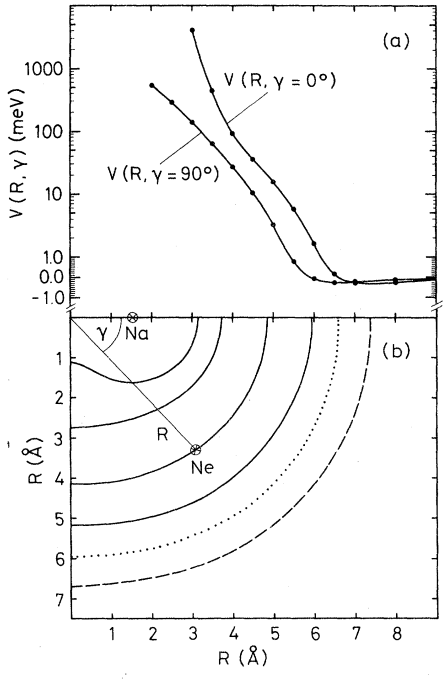

FIG. 3. (a) *Ab initio* interaction potential for $\gamma=0°$ and 90°. Full circles represent original energies (cf. Ref. 44). (b) Contour plot of the *ab initio* potential surface V_{CI}. Dashed line gives the position of the shallow van der Waals well (calculated well depth $\epsilon\cong 0.3$ meV) while the dotted line is the zero-energy contour. Beginning with the 2-meV contour the solid lines represent curves of constant potential with a factor of 10 increase in energy.

TABLE I. Parameters for the analytical expression of $V_{\mathrm{CI}}(R,\gamma)$ given by Eq. (3). Parameters a_i and b_i are in eV; a_2, c_i, and g_i are in Å^{-1}, d_i in Å^{-2}; e_i are in Å^{6}eV; and f_i and h_i in Å.

	$i=1$	$i=2$	$i=3$
a_i	5956.70	5.060 07	
b_i	3.096 67	0.517 869	0.382 472
c_i	0.573 842	−0.009 8666	0.565 999
d_i	0.114 477	0.154 557	0.098 6831
e_i	−41.882 1	3.651 35	
f_i	0.252 912	0.765 910	
g_i	1.743 95	0.032 2022	
h_i	2.092 75	−0.299 485	

Na_2. In this region the anisotropy of the potential gives rise to strong rotational excitation. According to the simple model of scattering from a hard shell[18,24] which in this case is an ellipsoid, the anisotropy is given by the difference of the semiaxes of the ellipsoid. For the present potential these differences are 0.70, 0.67, and 0.92 Å for collision energies of 20, 60, and 180 meV, respectively. At even shorter radial distances the third regime of the PES is observed. Here the penetration of the neon atom into the sodium molecule core region results in a much steeper repulsive interaction and large anisotropies.

The behavior described above is again demonstrated in Fig. 4, where the relative importance of the radial coefficients $V_\lambda(R)$ of the commonly used Legendre expansion of the interaction potential based on the global-fit expression are depicted. It is seen that for small radial distances the convergence of the expansion is slow and a large number of coefficients are needed to describe the potential. It is therefore not possible to attribute any physical significance to single V_λ expansion coefficients. As R is increased to intermediate values three or four coefficients $V_\lambda(R)$ are needed for a proper description. In the van der Waals region only two coefficients are sufficient.

The subsequent scattering calculations are not based on the global-fit expression Eq. (3) explicitly. Instead an interpolation scheme equivalent to that

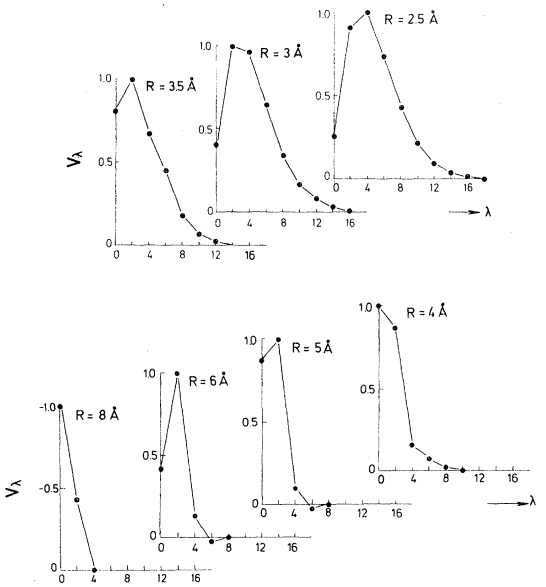

FIG. 4. Plot of the relative magnitude of the coefficients V_λ of the Legendre expansion for different radial distances R. In each case, the largest term has been normalized to unity.

described in detail previously for Na_2-He[47] is used. For each orientation angle γ_k, where *ab initio* energies $V_{CI}(R_i,\gamma_k)$ have been calculated, the R dependence is obtained by interpolating $\ln V_{CI}(R_i,\gamma_k)$ with a cubic spline function. The γ dependence of the potential is then determined by expanding $\ln V_{CI}(R_i,\gamma_k)$ into Legendre polynomials. Apparently, this procedure is applicable only for the repulsive branch of the interaction potential where V_{CI} is positive. The attractive part is treated differently. Here we expand the potential for each angle γ_k into a power series along the radial distance R and determine the coefficients by a linear least-squares procedure. Both branches of the potential are then smoothly matched. This representation of the potential surface reproduces exactly the calculated energies above 10 meV. Small deviations from the original energies due to the least-squares fit occur only in the region of the van der Waals well and the onset of the steep repulsion. This region has no noticeable influence on the scattering cross section for angles larger than $\theta_{c.m.}=5°$.

IV. SCATTERING THEORY

With the availability of the *ab initio* potential-energy surface one can perform the necessary scattering calculations to generate the rotationally inelastic differential scattering cross sections. It has been shown in Ref. 44 that rotational states up to $j\simeq 70$ must be included in the expansion of the total wave function. Therefore exact close-coupling calculations are not possible and an appropriate approximation must be made. An appealing choice is the infinite-order sudden approximation[48] which drastically reduces the computation time by effectively decoupling the full close-coupling system. This is accomplished by (a) replacing the orbital angular-momentum operator $\vec{l}$ by an average value $l(l+1)\hbar$ (centrifugal sudden approximation) and (b) replacing the molecular angular momentum operator j by an average value $j(j+1)\hbar$ [energy sudden (ES) approximation]. For excellent reviews of decoupling approximations see Ref. 49 and 50. Physically, the first part (a), also known as the coupled-states (CS) approximation,[51] assumes that the centrifugal potential is small as compared to the interaction potential. This is usually fulfilled for steeply repulsive, short-ranged potential-energy surfaces with shallow van der Waals minima as for the Na_2-Ne system. The second part (b) assumes that the amount of energy ΔE transferred to the molecule is much smaller than the collision energy E.

For the transitions experimentally studied here $\Delta E/E$ is less than 0.1. Thus the use of the ES approximation is justified. In fact it was found in Ref. 44 by comparing Na_2-Ne differential cross sections calculated in IOS and CS approximations for $E \leq 175$ meV that the former gives excellent results for those transitions studied in this work. Although CS calculations would in principle be feasible they would require about 150 times more computation time than the corresponding IOS calculation.[44]

Besides computational ease the IOS approximation offers a comprehensive explanation of rotational rainbows which can be regarded as the two-dimensional extension of the Ford and Wheeler analysis of rainbows in elastic atom-atom scattering.[52] This has been amply demonstrated[28–31,33,34] and only the basic aspects of the theory necessary to facilitate the interpretation of the Na_2-Ne data will be presented. As a starting point transitions out of the rotational ground state $j_i=0$ are considered.

Following Korsch and Schinke[33] the scattering amplitude for a $j_i=0$ to j_f transition at the scattering angle θ is written within the primitive semiclassical IOS approximation as

$$f(j_f \leftarrow 0 \mid \theta)=i(-1)^{j_f}2^{1/2}(k_{j_f}k_0\sin\theta)^{-1/2}\sum_{\gamma}[(l_\nu+\tfrac{1}{2})\sin\gamma_\nu/D(l_\nu,\gamma_\nu)]^{1/2}\exp[i\phi(l_\nu,\gamma_\nu)] \ . \tag{4}$$

In the above equation k_j is the wave number for channel j, γ is the orientation angle of the atom with respect to the molecular axis, and the phase is defined as

$$\phi(l,\gamma)=2\eta(l,\gamma)-(l+\tfrac{1}{2})\theta-(j_f+\tfrac{1}{2})\gamma \tag{5}$$

with $\eta(l,\gamma)$ being the γ-dependent elastic phase shift. The summation in Eq. (4) is over all roots (l_ν,γ_ν) of the coupled stationary phase equations

$$\theta(l,\gamma)\equiv 2\frac{\partial\eta(l,\gamma)}{\partial l}=\theta \ , \tag{6}$$

$$J(l,\gamma)\equiv 2\frac{\partial\eta(l,\gamma)}{\partial\gamma}=j_f+\tfrac{1}{2} \ , \tag{7}$$

and $D(l,\gamma)$ is the Jacobi determinant defined as

$$D(l,\gamma)=\left[\frac{\partial\theta}{\partial l}\right]_\gamma\left[\frac{\partial J}{\partial\gamma}\right]_l-\left[\frac{\partial\theta}{\partial\gamma}\right]_l\left[\frac{\partial J}{\partial l}\right]_\gamma \ . \tag{8}$$

Equation (4) is derived under the following assumptions. First, the molecule is homonuclear. Second, the functions $\theta(l,\gamma)$ and $\partial\theta(l,\gamma)/\partial l$ are nonzero and positive for all l and γ. Third, the excitation function $J(l,\gamma)\geq 0$ for all l within the range $0\leq\gamma\leq\pi/2$. The latter two assumptions are usually fulfilled for impulsive collisions. In particular they are valid for the Na_2-Ne system (see Fig. 3 of Ref. 44).[53]

Since in the present case the experimental differential cross sections are available as angular distributions for fixed transitions j_i to j_f, one solves Eq. (7) for l with fixed j_f. This procedure defines a contour $l=l(\gamma \mid j_f)$ which when inserted into Eq. (6) establishes the γ-dependent deflection function for the chosen transition, i.e., $\theta(\gamma \mid j_f)=\theta(l(\gamma,j_f),\gamma)$ which should not be confused with the deflection function previously defined in Eq. (6). Characteristic examples of $\theta(\gamma \mid j_f)$ are presented in Fig. 5(a). Each curve has a minimum angle $\theta_R(j_f)$ which is an increasing function of j_f. This behavior can be explained by considering the γ dependence of the excitation function $J(l,\gamma)$ which because of symmetry must be zero when $\gamma=0$ or $\pi/2$. Thus the function $J(l,\gamma)$ must have a maximum in the closed interval at some angle γ_R. The maximum value of J at γ_R decreases with increasing l. Holding j_f fixed restricts l and results in a restricted range of $\theta(\gamma \mid j_f)$.

From Fig. 5(a) one also observes that, for a given pair (θ,j_f), two points of stationary phases γ_1 and γ_2 contribute to the scattering amplitude which are real for $\theta>\theta_R(j_f)$ and conjugate complex for $\theta<\theta_R(j_f)$. The primitive semiclassical IOS cross section in the classically allowed range $[\theta>\theta_R(j_f)]$ is then given by[33,54]

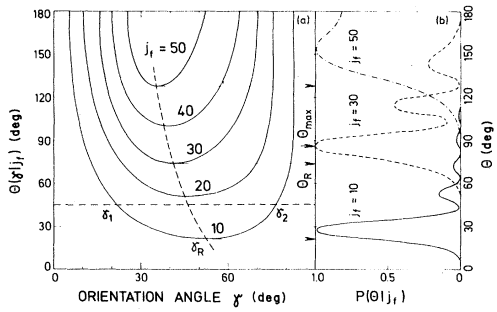

FIG. 5. (a) Deflection function $\theta(\gamma \mid j_f)$ as a function of the orientation angle γ of the molecular axis with respect to the incoming particles. Deflection function is plotted for various values of the momentum transfer j_f. Dashed line indicates the rainbow curve $\theta_R(\gamma_R \mid j_f)$. (b) Relative IOS differential cross sections for $j_f=10$, 30, and 50 as a function of scattering angle.

$$\sigma(j_f \leftarrow 0 \mid \theta) = 2(k_0^2 \sin\theta)^{-1}[F_1^2 + F_2^2 + 2F_1F_2\sin(\phi_1 - \phi_2)] , \quad (9)$$

where the classical probabilities F_v are defined as

$$F_v = [(l_v + \tfrac{1}{2})\sin\gamma_v / \mid D(l_v,\gamma_v) \mid]^{1/2} \quad (10)$$

and $\phi_v = \phi(l_v,\gamma_v)$. In the classically forbidden range $[\theta < \theta_R(j_f)]$ the cross section is given by

$$\frac{d\sigma}{d\Omega}(j_f \leftarrow 0 \mid \theta) = 2(k_0^2 \sin\theta)^{-1} F^2 \exp(-2 \mid \mathrm{Im}\phi \mid) , \quad (11)$$

where $\mid F \mid = \mid F_1 \mid = \mid F_2 \mid$ and $\mid \mathrm{Im}\phi \mid = \mid \mathrm{Im}\phi_1 \mid = \mid \mathrm{Im}\phi_2 \mid$.

If the Jacobian determinant $D(l_v,\gamma_v)$ is zero at a point (l_R,γ_R), then the cross section becomes singular. Since it has been assumed that $(\partial\theta/\partial l)(l,\gamma) \neq 0$ is true for all (l,γ) it is easy to show that $D(l_v,\gamma_v) = 0$ is equivalent to the condition $(d\theta/d\gamma)(\gamma \mid j_f) = 0$. The coalescence of the two stationary phase angles γ_1 and γ_2 at the minimum angle $\theta_R(j_f)$ produces the so-called *rotational rainbow.*[55] Improved cross sections are obtained with an Airy-type uniform analysis[33] which replaces the unphysical singularity with a maximum at $\theta_{\max}(j_f)$ shifted to greater angles than $\theta_R(j_f)$.

In Fig. 5(b) are plotted a series of cross sections, normalized to unity at the rainbow maximum, as a function of scattering angle θ. Each cross section exhibits a distinct maximum at the angle $\theta_{\max}(j_f) > \theta_R(j_f)$. To smaller angles the cross sections rapidly decrease towards zero as a result of increasing $\mid \mathrm{Im}\phi \mid$ in Eq. (11). To greater angles the cross sections decrease more or less slowly due to the $(\sin\theta)^{-1}$ dependence. The *supernumerary rotational rainbows,* i.e., the secondary maxima in the cross sections, stem from the interference term in Eq. (10). If a $0 \rightarrow j_f$ transition is classically forbidden at all angles the differential cross section rises monotonically with θ without showing any further structure. One observes also that $\theta_{\max} - \theta_R$ is an increasing functin of j_f.

The dependence of the rainbow angles θ_R upon j_f, the potential-energy surface, and the wave number k is given by[56]

$$\theta_R = 2\sin^{-1}(j_f / 2k\Delta) \quad (12)$$

derived within the classical model of scattering from a hard potential shell. Here k is the wave number $(2\mu E)^{1/2}$ with μ the collision-system reduced mass and Δ is a constant which depends only on the potential-energy surface. In the case that the potential shell is an ellipsoid Δ is given by the difference in length of the ellipsoids long and short half-axes.[27(a)] It is shown in Ref. 44 for the Na_2-Ne system that Eq. (12) provides an adequate approximation of the quantal curve $\theta_{\max}(j_f)$. Thus a knowledge of the rainbow angles $\theta_{\max}(j_f)$ from the experiment leads to an approximate but straightforward determination of the anisotropy of the potential.[18]

Although the theory has been presented considering the initial state to be $j_i = 0$, the generation of cross sections from states with $j \neq 0$ is facilitated through the use of the factorization formula for fixed collision energy

$$\frac{d\sigma}{d\Omega}(j_f \leftarrow j_i \mid \theta) = \sum_j C^2(j_i j j_f \mid 000) \frac{d\sigma}{d\Omega}(j \leftarrow 0 \mid \theta) . \quad (13)$$

This result has been derived by various authors[57] and results from the energy-sudden part of the IOS approximation.[58] The theoretical cross sections for transitions $j_i \rightarrow j_f$ with j_i and $j_f \neq 0$ have been constructed using Eq. (13) and will be compared to the experimental results in Sec. V along with a more complete discussion of the general form of rotationally inelastic differential cross sections.

V. CENTER-OF-MASS TRANSFORMATION OF THE EXPERIMENTAL CROSS SECTIONS

Transformation of the theoretical data from the center-of-mass frame into that of the laboratory system requires a detailed knowledge of the experimental detection system in order to properly average the theoretical cross section over the experimental resolution. This procedure is unambiguous but the resulting cross sections are convoluted with the experimental angular resolution function. Transformation of the experimental data to the center of mass deconvolutes the angular resolution function and the cross section. In most cases, however, this transformation is ambiguous and decreases the precision of the data. Various techniques are available for dealing with the mechanics of the transformation and the fact that the transformation is multivalued.[59] The method employed here, Monte Carlo simulation of the transformation matrix followed by a constrained minimalization fitting procedure to determine the c.m. cross section, has been developed in order to introduce the least possible bias into the transformation procedure.[60]

The laboratory count rate $N(\theta_{\rm lab})$ of the experiment can be related to the c.m. cross section $\sigma(\theta_{\rm c.m.})$ by

$$N(\theta^s_{\rm lab})=\beta\sum_r R(\theta^s_{\rm lab},\theta^r_{\rm c.m.})\sigma(\theta^r_{\rm c.m.})\ , \tag{14}$$

where β is the factor relating count rates to cross sections and R is a matrix which includes the Jacobian of the transformation between frames as well as the angle-dependent detection probability set by the experimental conditions. Using the measured beam velocity distributions and other known experimental factors, the matrix R is determined through a Monte Carlo simulation. The transformation matrix elements for three laboratory angles are drawn in Fig. 6. The laboratory angle of $\theta_{\rm lab}=40°$ is mapped into an angle interval of close to $\Delta\theta_{\rm c.m.}=50°$ in the c.m. frame. Examination of the full transformation matrix shows that in the range below roughly 30° laboratory angle the transformation is dominated by forward scattering in the c.m. frame and small angular regions in the laboratory map into small angular regions in the center of mass.

The set of cross sections is determined by minimizing

$$\chi^2=\sum_s\left[\frac{N(\theta^s_{\rm lab})-N^e(\theta^s_{\rm lab})}{\Delta N^e(\theta_{\rm lab})}\right]^2, \tag{15}$$

with $N(\theta^s_{\rm lab})$ substituted according to Eq. (14), subject to the physical constraint that $\sigma(\theta^r_{\rm c.m.})\geq 0$. Because of the limited angular resolution each $\sigma(\theta^r_{\rm c.m.})$ is an average over the angular interval $\Delta\theta_{\rm c.m.}=6°$, except for backward scattering (see Fig. 6). The experimentally measured values of the count rate at angle $\theta^s_{\rm lab}$, $N^e(\theta^s_{\rm lab})$ have an error given by $\Delta N^e(\theta^s_{\rm lab})$. The error of the cross section $\sigma(\theta^r_{\rm c.m.})$ is determined by repeating the minimalization procedure with random variation of N^e and R assuming a Gaussian distribution according to their statistical error.

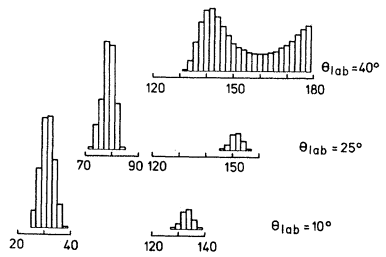

FIG. 6. Elements of the transformation matrix $R(\theta_{\rm lab}, \theta_{\rm c.m.})$ between the laboratory and c.m. frames for laboratory angles $\theta_{\rm lab}=10°$, 25°, and 40°, respectively. Horizontal scale gives $\theta_{\rm c.m.}$.

This transformation procedure avoids the use of a parametrized model function and provides a realistic estimate of the error in the relative magnitude of the resulting c.m. cross section.

A trial transformation (Fig. 7) provides an example of the accuracy of the method. Figure 7(a) shows a c.m. cross section (solid line) similar to that for the $j_i=9$ to $j_f=29$ transition. In Fig. 7(b) the solid line represents the theoretical curve after transformation into the laboratory frame; the points in Fig. 7(a) are the results of the transformation of this curve back to the c.m. system. After adding random noise to the simulated laboratory data [points in Fig. 7(b)] the noisy curve is transformed into the center-of-mass frame. The boxes in Fig. 7(c) represent the transformed data and give the estimated angular uncertainty and 1σ statistical uncertainty in the transformed intensity. The solid line in Fig. 7(c) is the original curve. As a final check the transformed data is retransformed into the laboratory frame and compared against the original simulated data [Fig. 7(d), open and full circles, respectively]. Exact reproduction of the original theoretical curve is not expected due to the presence of noise in the data. Although finer details are

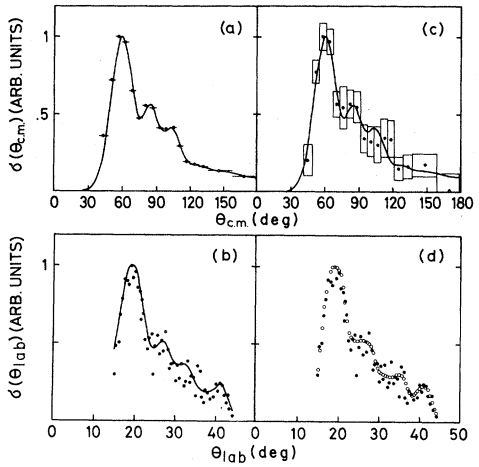

FIG. 7. Test of the transformation procedure. Solid line in (a) is similar to the calculated $j_i=9\rightarrow j_f=29$ center-of-mass cross section. It is transformed to the laboratory frame using Eq. (14) [solid line (b)]. The result of the transformation back into the c.m. frame is given by the dots in (a). After adding representative noise to the laboratory data [dots in (b)] the curve is transformed to the c.m. frame [dots and boxes in (c)] and shown together with the original cross section [solid line in (c)]. Noisy c.m. data (c) are finally transformed back to the laboratory system and compared with the original noisy laboratory curve [open and filled circles, respectively, in (d)].

averaged out the general form of the cross section has been well reproduced. Since the matrix R is known only to within the accuracy of the input data and simulation procedures, an additional error not inherent to the statistical error of the count rate occurs when the transformation is made. This additional error tends to be systematic and mainly affects the region of large c.m. scattering angles[61] (see Fig. 6).

VI. RESULTS AND DISCUSSION

A. General form of the differential cross sections

The present experiment measures the differential cross section for fixed angular momentum change Δj as a function of scattering angle θ. The experimental data transformed into the c.m. frame are presented in Figs. 8, 9, 11, and 12. As in Fig. 7 the boxes represent the transformed experimental data and the appropriate uncertainty in angle and intensity while the solid curves are the IOS cross sections calculated using the potential surface described in Sec. III. The curves are given in arbitrary units each normalized to unity at the rainbow maximum. The proper relative scaling of the experimental cross sections will be discussed in Sec. VI C. From the discussion in Sec. IV one expects the cross sections to be divided into two zones. A classically forbidden region at angles less than θ_R and the classically allowed region from θ_R to 180° c.m. In the classically forbidden region the cross section is small and tends to zero as θ approaches zero. As the scattering angle is increased past θ_R the value of

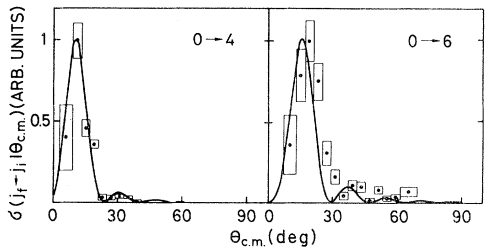

FIG. 8. Differential c.m. cross sections for transitions $j_i=0$ to $j_f=4$ and $j_i=0$ to $j_f=6$. Dots are experimental data. Cross sections are an average over the angular interval given by the width of boxes. Error in the cross section, as determined by the procedure described in Sec. V, is represented by the height of the boxes. It is equivalent to one standard deviation. Solid lines are cross sections calculated in IOS approximation using the *ab initio* potential-energy surface.

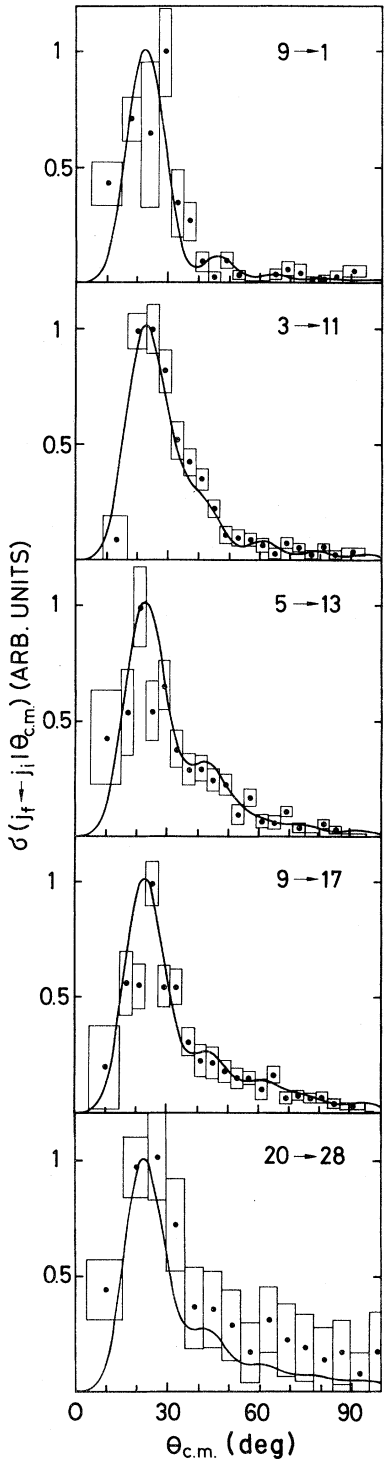

FIG. 9. A sequence of c.m. cross sections for transitions with $\Delta j=8$ and $j_i=1$ to 20. The $j_i=20$ to $j_f=28$ cross section is taken from Ref. 14. Notation is the same as in Fig. 8.

the cross section rises steeply to a maximum value at the angle θ_{max} and then declines nonmonotonically towards 180°. This behavior is exhibited by all the experimental cross sections shown here and is well documented.[34]

The physical basis of this behavior has been discussed in Sec. IV. It is also easily understood within the classical model of point scattering from rigid rotationally symmetric shells as developed by Beck *et al.*[24,25] For a given Δj and anisotropy, collisions leading to angles less than θ_R do not exert the necessary torque to make the transition Δj because the effective force exerted normal to the shell during the collision is inadequate. As Δj increases, the amount of torque necessary to make the transition increases, forcing θ_R to shift to larger values.

From the deflection functions $\theta(\gamma \mid j_f)$ plotted in Fig. 5(a) and the corresponding cross sections in Fig. 5(b) one expects that with increasing Δj the maximum in the differential cross section should broaden and lose intensity with respect to the scattering at larger angles. The experimental cross sections exhibit precisely the expected trends. Finer details of the experimental cross sections are examined in the next section.

B. Specific forms of the differential cross sections

1. *Cross sections with* $j_i=0$

The theoretical cross sections for transitions involving $j_i=0$ all show oscillations as a result of the interference between scattering events which end in identical states but involve scattering from different molecular orientations.[34] As the initial rotation of the molecule is increased the structure loses distinctness due to the increasing range of initial m sublevels whose cross sections sum to the total with different phases.[44] Therefore the best experimental probe for the presence of the supernumerary rainbows is from cross sections with $j_i=0$.

Three experimental cross sections with $j_i=0$ are shown in Figs. 2 and 8. The $j_i=0$ to $j_f=2$ cross section could not be transformed into the c.m. frame as a result of the large change in intensity over a very small angular range which leads to numerical instability in the transformation procedure. The rainbow maximum is also absent in this curve since its angular position lies within the primary beam profile. It is also not observable in the theoretical $j_i=0$ to $j_f=2$ cross section because it occurs at very small scattering angles and is therefore buried under the forward diffraction peak. However, the experimental cross section shows clearly the first supernumerary maximum and indications of the second. In the $j_i=0$ to $j_f=4$ cross section the rainbow maximum is resolved but instead of a clear supernumerary maxium the experimental curve shows only a leveling off in the cross section in the range of angles where this maximum is expected to occur. For the $j_i=0$ to $j_f=6$ transition the noise in the cross section is sufficient to preclude any definite statement concerning the presence of supernumerary structure. In all cases the theoretical curves correctly describe the measured cross sections.

Besides the presence of supernumerary rainbows these cross sections illustrate the strong forward peaking of cross sections for small Δj transitions in the Na_2-Ne system. At angles greater than 15° laboratory, the elastic scattering intensity is undetectable,[14] implying that scattering into larger angles results from inelastic events. This trend is mirrored in the inelastic cross sections and underlines the strong coupling of rotational levels in this system. The small angular width of the rainbow maximum also demonstrates the strong correlation between a small range of initial orbital angular momentum values and rotational transitions Δj.

2. *Cross sections for* $\Delta j=8$.

Another interesting aspect of rotationally inelastic collisions is the dependence of the cross section for fixed Δj on the initial rotation j_i. While varying j_i one probes also the influence of energy exchange versus momentum transfer. Figure 9 shows five cross sections for $\Delta j=8$ which differ in initial and final states. The energy exchanged varies a factor of 4.4 over the range of initial and final states investigated. One sees immediately from Fig. 9 that the dominant feature of the cross section, namely the rainbow maximum, has the same angular position to within experimental error in all five cross sections. This illustrates that the dynamical constraint concerns the momentum transfer and not the energy transfer, in accordance with expectations. This behavior has also been found theoretically for transitions with Δj up to 40.[44] Finer details of the cross sections in Fig. 9 are, however, different and provide information concerning the role of initial and final states in determining the form of the cross section. One notices, for example, that as j_i increases the scattering intensity to larger c.m. angles increases relative to the intensity at the rainbow max-

imum. Within the sudden approximation the molecule is assumed to be nonrotating on the time scale of the collision. Therefore the initial and final rotational states are important only insofar as they set the value of the range and number of contributing m_i levels and of possible Δm transitions.

Figure 10 illustrates the quantum-state dependence of the cross sections by presenting a series of theoretical $\Delta j=8$ IOS cross sections calculated with the help of Eq. (13). The intensity scale is logarithmic and given in absolute units. For the $j_i=0$ to $j_f=8$ cross section, the quantum oscillations are clearly visible. With increasing j_i the oscillatory structure is damped but interestingly enough *not* absent. The arrow gives the angular position of the rainbow maximum $\theta_{\max}(j)$ of the largest $0\rightarrow j$ transition contributing according to Eq. (13). In this angular range the regular oscillatory structure is slightly distorted. The cross section for backward scattering is almost constant independent of j_i while the cross section at the rainbow maximum decreases with increasing j_i. These trends are nicely documented by the experimental curves in Fig. 9.

3. *Cross sections for excitation and deexcitation*

The four cross sections presented in Fig. 11 along with those for $j_i=9$ to $j_f=1$ and 17 in Fig. 9 represent a set of excitation/deexcitation cross sections from a common initial level $j_i=9$. Those shown cover the range $\Delta j=\pm 8,\pm 6,\pm 4$. Provided the orientation of the molecule in j_i is isotropic, microreversibility requires the form of the cross sections j_i to j_f and j_f to j_i to be identical within the

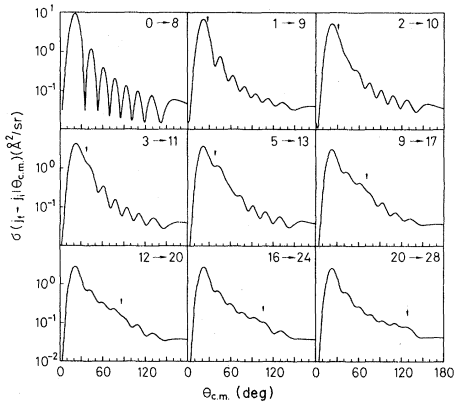

FIG. 10. IOS differential cross sections for $\Delta j=8$ transitions and a variety of initial rotational levels j_i. Collision energy is 190 meV. Arrows indicate the angular position $\theta_{\max}(0\rightarrow j)$ for the largest j contributing in Eq. (13).

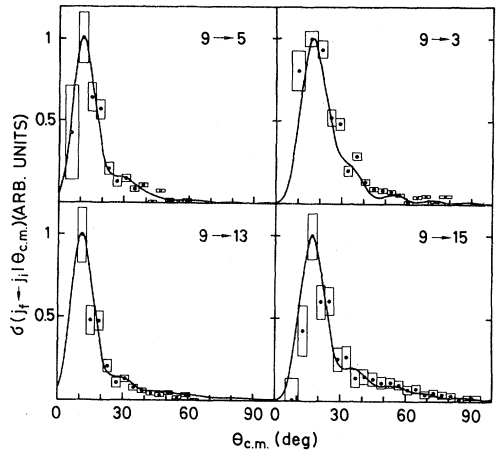

FIG. 11. Excitation and deexcitation c.m. cross sections for $\Delta j=\pm 4$ and ± 6 from the initial rotational level $j_i=9$. Notation is the same as in Fig. 8.

energy-sudden limit. This is easily seen by inspection of Eq. (13) and the symmetry relation

$$(2j_i+1)C^2(j_ijj_f\,|\,000)=(2j_f+1)C^2(j_fjj_i\,|\,000)\ .$$

Therefore this set contains additional evidence for the dependence of the cross section for fixed Δj on j_i as discussed above. The relative increase of the cross section at larger scattering angles with increasing j_i is most clearly seen when comparing the $j_i=1$ to $j_f=9$ and $j_f=9$ to $j_f=17$ transitions. It is also observable although less obvious for the $|\Delta j|=6$ and $|\Delta j|=4$ transitions.

4. *Cross sections for* $\Delta j=12$, *14, 16, and 20*

The cross sections for the largest Δj transitions studied are presented in Fig. 12. These cross sections provide another clear representation of the general trends to be expected in the rotationally inelastic differential cross sections for impulsive scattering from steeply repulsive potentials as discussed in Sec. IV. As Δj is increased the angular positions of the rainbow maxima shift to greater c.m. angles. The maxima themselves become less distinct and the scattering intensity in the backward direction relative to that of the maximum increases as Δj increases. The clear division of the cross sections into dark and bright zones by the rainbow maxima is, however, observed. Although the experimental data lie above that calculated at large scattering angles, the agreement between the form of the theoretical and experimental cross sections is

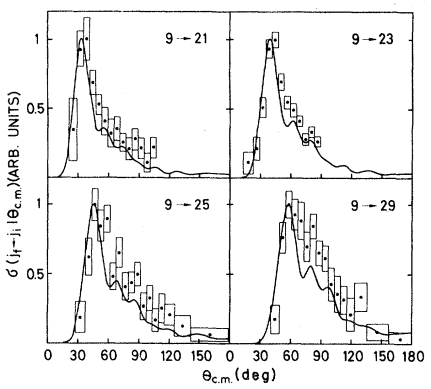

FIG. 12. Differential c.m. cross sections for relatively large Δj transitions. Notation is the same as in Fig. 8.

good. A reason for the discrepancy in magnitudes could not be identified unambiguously. It has been shown in Ref. 44 for a collision energy of 175 meV that the cross sections calculated in CS approximation are slightly larger than the IOS cross sections for backward scattering and the range of Δj transitions relevant here. Comparison with CS results could therefore reduce but not eliminate the remaining discrepancy. It is also expected that the error in the IOS and CS approximation made by forcing the orbital angular momentum to be constant increases with increasing Δj and contributes to the observed discrepancy. Since the theoretical and the experimental rainbow positions agree very well within the experimental uncertainty we are confident that the overall anisotropy of the *ab initio* potential is correct. We cannot exclude, however, that minor uncertainties in the curvature especially in the vicinity of the rainbow orientation angle γ_R, which in turn affect the form of the rainbow maximum,[33] could be made responsible for the observed deviation. Finally it has been noted in Sec. V that errors in the transformation matrix R [see Eq. (14) and Fig. 6] affect mainly the cross sections at large scattering angles.

C. Relative magnitudes of the differential cross sections at $\theta_{max}(\Delta j)$

The relative magnitudes of the experimental cross sections can be compared if one knows the relative populations of the initial states. The latter have been determined by measuring the relative fluorescence intensities under identical experimental conditions and with measured laser intensity.[41] The theoretical curves are available as absolute cross sections and their magnitudes can be compared to those of the experimental cross sections if the two are normalized to one another at a single point. The point chosen is the peak of the $j_i=9$ to $j_f=13$ cross-section curve. The results have been tabulated along with a summary of the rainbow maximum angles in Table II. The presentation of the experimental cross sections in absolute units is based upon the results of the calculations and they should not be mistaken for experimentally verified numbers; the experiment measures only relative cross sections. The tabulated results show that not only the angular position θ_{max} of the rainbow maximum but also the relative magnitudes of the theoretical and experimental cross sections at θ_{max} agree to within the experimental uncertainty.

D. Relative magnitude of integral cross sections

We conclude this section with the discussion of integral cross sections since these are the quantities needed to model rotational relaxation in a gas. Integral $\sigma(j_f \leftarrow j_i)$ IOS cross sections are given in the last column of Table II. The *relative magnitude* of these numbers can be considered as experimentally verified since the angular variation of the calculated cross sections and their relative magnitude at θ_{max} agree well with the experimental data. For a fixed Δj the differential cross section $\sigma(j_f \leftarrow j_i \mid \theta_{max})$ decreases faster with j_i than does the integral cross section $\sigma(j_f \leftarrow j_i)$. Thus we observe a decreasing transition probability as well as a redistribution of scattering intensity towards larger scattering angles as j_i increases (see also Figs. 9 and 10). Figure 13(a) summarizes a large set of calculated cross sections. The individual curves are labeled by Δj. The solid lines are obtained by interpolating cross sections for different j_i with $0 \le j_i \le 24$. Circles and squares are used for $j_i=0$ and 24, respectively. The triangles correspond to experimentally verified relative cross sections (see Table II). It is interesting to note that the integral cross section decreases more rapidly with j_i as Δj increases [$\sigma(4\leftarrow 0)/\sigma(28\leftarrow 24)=1.62$, $\sigma(24\leftarrow 0)/\sigma(48\leftarrow 24)=2.25$].

The set of data is is presented again in Fig. 13(b) normalized according to the statistical power-gap law[62] which in many cases is found to be superior to the previously derived exponential gap laws.[63] Such fitting laws have been derived and tested with the goal to describe a large set of cross sections or rate constants with a small set of parameters. It has been found in Ref. 62 that a fit procedure based on the energy corrected sudden scaling law[64] gave in

TABLE II. Comparison of measured and calculated cross sections and angular positions of rainbow maxima for $E = 190$ meV.

Transition $j_i \rightarrow j_f$	Δj	θ_{max}^{exp} (deg)	θ_{max}^{IOS} (deg)	$\sigma^{exp}(j_f \leftarrow j_i \mid \theta_{max})$ (Å^2/sr)	$\sigma^{IOS}(j_f \leftarrow j_i \mid \theta_{max})$ (Å^2/sr)	$\sigma^{IOS}(j_f \leftarrow j_i)$ (Å^2)
0—4	4	11	10.5	35.0	36.5	10.44
5—9	4	11	11	15.1	15.2	7.93
9—13	4	11	11	13.7[a]	13.7	7.35
24—28	4	b	11	b	11.4	6.45
0—6	6	19	16	15.1	16.0	7.79
3—9	6	16	17	8.8	7.75	6.44
9—15	6	17	17	6.0	5.68	5.46
1—9	8	29	22.5	5.2	6.64	5.85
3—11	8	24	22.5	5.3	4.35	5.30
5—13	8	21	22.5	4.1	3.58	4.94
9—17	8	25	22.5	3.2	3.04	4.38
20—28	8	24	22.5	2.7	2.6	3.70
9—21	12	36	34	1.2	1.25	3.09
16—28	12	37	34	1.1	1.0	2.67
9—23	14	42	40	1.0	0.89	2.65
9—25	16	46	45.5	1.0	0.67	2.29
12—28	16	47	45.5	0.6	0.6	2.11
8—28	20	61	57.5	0.4	0.4	1.75
9—29	20	58	57.5	0.5	0.4	1.69
4—28	24	70	69	0.35	0.3	1.50

[a]The experimental cross sections are normalized to the calculated ones at this point.
[b]Not measured.

general slightly better fits. When the collisions are truly sudden, as in the present case, both approaches lead to identical results. All reduced cross sections fall near a single line, i.e., the variation of the cross section with j_i and Δj for a given ΔE is surprisingly well described by the factor $k_i/(2j_f+1)k_f$. The ratio of wave numbers $k=(2\mu E)^{1/2}$ assures that the cross sections obey microreversibility, while applying the factor $(2j_f+1)$ is equivalent to the assumption of a random orientation of j_f. It has been pointed out in Ref. 64, however, that the quality of a fitting law is an unreliable criterion for the test of dynamical features of the process and the interaction potential.

Obviously the reduced cross sections do not fall on a *straight* line. This has been observed previously for cross sections in Na_2-Ne, He (Ref. 65) as well as He-LiH (Ref. 66) and H_2-CO_2 (Ref. 67) scattering. It has been shown in Ref. 64 that classically forbidden transitions are characterized by a significantly larger exponent γ when fitting the variation of the reduced cross sections σ_r according to $\sigma_r \simeq \Delta E^{-\gamma}$. In the present case the slope changes significantly near $\Delta E = 10$ meV or $\Delta E/E \simeq 0.05$. From a least-squares fit we find $\gamma = 0.97$ for $\Delta E \leq 10$ meV and $\gamma = 1.32$ for $\Delta E > 10$ meV. The former value is very close to that one reported in Ref. 62 for rotational energy-transfer-rate constants of *electronically excited* Na_2 colliding with Ne.

VII. SENSITIVITY ANALYSIS

The comparison of the theoretical and experimental cross sections has shown that within the experimental uncertainty the IOS cross sections calculated from the *ab initio* potential-energy surface provide an accurate representation of the experimental results. Although one expects the IOS approximation to be valid at the 190-meV collision energy for the transitions investigated in the present study the good agreement between theory and experiment is surprising. In this section we attempt to determine the extent to which the calculated potential surface is verified by the experiments, i.e., the sensitivity of the agreement with respect to a variation of anisotropy, steepness, R shift, and well depth as the main parameters of the potential.

The variation of the *ab initio* potential in a way which allows one to vary the parameters independently is somewhat difficult. In the weak-coupling case, where only two terms of an expansion into

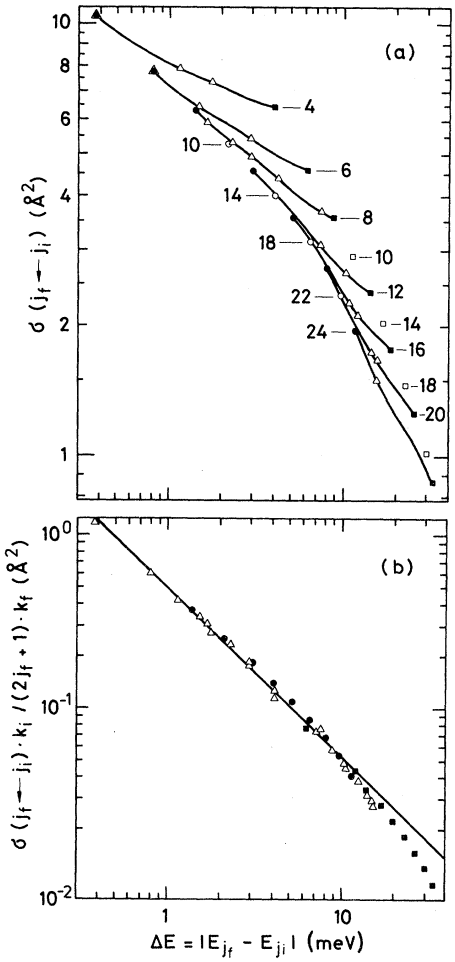

FIG. 13. (a) Variation of the calculated integral cross section $\sigma(j_f \leftarrow j_i)$ as j_i and Δj change. Solid lines, labeled by Δj, are obtained by interpolating cross sections for different initial rotational levels j_i with j_i varying from $j_i=0$ (circles) to $j_i=24$ (rectangles). For some Δj transitions only the cross sections out of $j_i=0$ and $j_i=24$ are given (open circles and rectangles, respectively). Triangles correspond to experimentally verified relative cross sections (see Table II and Sec. VI D). (b) Variation of the reduced cross sections $\sigma(j_f \leftarrow j_i)k_i/[(2j_f+1)k_f]$ with change in rotational energy ΔE. Only the cross sections for $j_i=0$ and $j_i=24$ as well as those experimentally verified are included. Symbols are the same as in (a).

Legendre polynomials V_0 and V_2 have to be considered, the single coefficients can be varied separately and their influence on the elastic and inelastic cross section can be investigated. Such a study has been performed for Ne-HD.[68] This is not possible in the present case where many terms V_λ have to be included. It is also difficult to use the global-fit expression Eq. (3) for an independent variation of anisotropy and steepness of the potential-energy surface which will be discussed first. The method chosen here is to multiply the analytical potential expression as used in the scattering calculations by either an angular or radial function $p(\gamma)$ or $q(R,\gamma)$, respectively, with a variable strength parameter, i.e.,

$$V(R,\gamma)=V_{\rm CI}(R,\gamma)\begin{cases}p(\gamma), & \text{(16a)}\\ q(R,\gamma)\ . & \text{(16b)}\end{cases}$$

$V(R,\gamma)$ is the resulting varied potential-energy surface.

Before specifiying the functions p and q it is necessary to define the terms "anisotropy" and "steepness" of the potential. Inspection of Fig. 3(a) suggests to approximate the *ab initio* potential for intermediate radial distances by the simple model expression

$$V_{\rm mod}(R,\gamma)=e^{-\alpha(R-R_0)}[1+\beta P_2(\cos\gamma)]\ . \quad (17)$$

The three parameters $\alpha=1.683$ Å^{-1}, $\beta=0.8710$, and $R_0=2.141$ Å are obtained by fitting the above expression to the original potential energies between 10 and 200 meV. Obviously, Eq. (17) does not reproduce finer details of the potential-energy surface. It is, however, a realistic representation of the *ab initio* potential for the region of intermolecular separations that are mainly probed in the experiment. Here $\beta=V_2/V_0$ defines the anisotropy and the slope parameter α is called the steepness. This simple model potential gives angular positions of the rotational rainbows slightly below those obtained experimentally. For $\Delta j=20$ the maximum is found near $\theta_{\rm c.m.}=52°$ which is slightly outside the experimental error bars (see Table II). The parameters of the model potential Eq. (17) are, however, only used as reference for the parameters to be varied in Eq. (16).

The angular variation function is chosen as

$$p(\gamma)=1+\Delta\beta P_2(\cos\gamma) \quad (18)$$

and $\Delta\beta$ is varied between -25% and 25% with respect to β. The isotropical part of the *ab initio* potential, which mainly determines the semiclassical relation between the scattering angle and the orbital angular-momentum parameter,[44] remains unchanged. The radial variation function is chosen to be

$$q(R,\gamma)=e^{-\Delta\alpha[R-R_t(\gamma)]} \quad (19)$$

and $\Delta\alpha$ is varied between -25% and 50% with

respect to α. The function $R_t(\gamma)$ is the contour line of classical turning points for an intermediate orbital angular momentum $l=90\hbar$ for which the $\Delta j=20$ partial cross section reaches its rainbow maximum. The appearance of $R_t(\gamma)$ instead of an average, angular independent value of R in the exponent of Eq. (19) assures that the potential contours which mainly determine the positions of the rotational rainbows for the highest transitions resolved in the experiment remain unaltered. According to the model of scattering from a hard shell, Eq. (12), it is the shell contour which exclusively determines the angular positions of rotational rainbows for a fixed collision energy.

The sensitivity of the scattering calculation on the potential-energy surface is investigated by comparison of the quantal rainbow angles $\theta_{\max}(\Delta j)$ obtained from the varied potentials with those obtained from the original potential $V_{\rm CI}(R,\gamma)$ and those determined experimentally. The sensitivity is expected to be largest in the rainbow region where the classical cross section tends to infinity. The IOS calculations are performed at the experimental collision energy $E=190$ meV with $j_i=9$.

The variation of the angular position of the rainbow maximum $\theta_{\max}(\Delta j)$ with the anisotropy is plotted in Fig. 14(a). Each of the family of curves gives the location of the rainbow maximum for differing Δj transitions and a particular value of $\Delta\beta$. First one observes that all curves can be quite well represented by the simple formula given in Eq. (12) that predicts a linear increase of $\theta_{\max}$ with Δj for sufficiently small angles. The anisotropy decreases as one changes $\Delta\beta$ from 25% to -25%. The experimental results and the curve for $\theta_{\max}$ which results from the original, unvaried potential $V_{\rm CI}$ are also plotted. From the Figure one sees that the experimental results are consistent with those calculated only if the anisotropy of the *ab initio* potential is accurate to within approximately $\pm 5\%$.

The variation of $\theta_{\max}(\Delta j)$ as the steepness of the potential is changed is given in Fig. 14(b). Again the results from the experiment and the unvaried potential are illustrated for comparison. It is apparent that the rainbow angular positions are relatively insensitive to the steepness of the potential. A variation of the steepness α of the potential by no more than -10% or $+25\%$ would still lead to an acceptable agreement with the experimental data. As α increases the angular rainbow position becomes less sensitive to the steepness of the potential. In the limit of very large α the potential surface approaches that of a hard shell and the rainbow position is determined by the difference of the semilong and semishort axis alone.

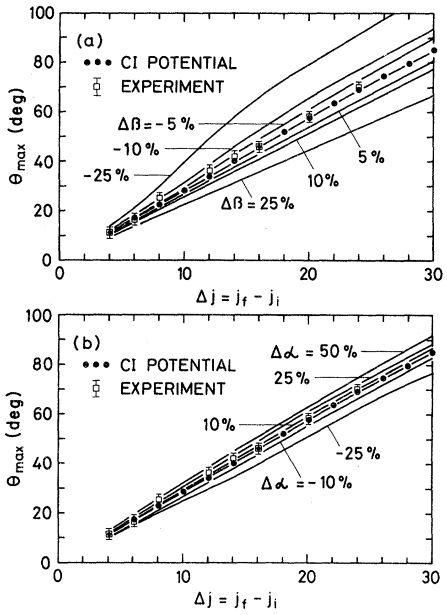

FIG. 14. Variation of the angular position of the rainbow maximum $\theta_{\max}(\Delta j)$ as the anisotropy (a) and the slope (b) of the interaction potential are varied. Curves for a variety of parameters $\Delta\beta$ and $\Delta\alpha$ as defined in Eqs. (18) and (19) are shown together with the results from the original *ab initio* interaction potential $V_{\rm CI}$ and the experimental data. Collision energy is 190 meV and $j_i=9$, except for $\Delta j=24$ where $j_i=4$.

Figure 15 illustrates the dependence of the intensity of the cross sections $j_i=9$ to j_f at the angle $\theta_{\max}(\Delta j)$ on the variations in anisotropy and steepness of the potential. All curves are normalized to the intensity of the $j_i=9$ to $j_f=13$ transition as obtained from the original surface $V_{\rm CI}$. One sees that the intensity of the cross section at $\theta_{\max}$ is an unreliable guide to the accuracy of the potential and that more data with higher precision and a greater range of rotational transitions would be needed to make quantitative conclusions. The general trends are however consistent with those deduced from the results plotted in Fig. 14.

Besides the anisotropy and the steepness of the interaction potential discussed so far, a shift in the radial distance R and the well depth of the van der Waals minimum have been considered. Both variations proved, however, to be very insensitive with respect to the experimental results. Shifting the entire potential by $\Delta R=\pm 0.06$ Å, which is twice the claimed maximum uncertainty of the *ab initio* potential in the repulsive wall, does not change the calculated curve of rotational rainbows. Increasing the well depth by as much as a factor of 10 but

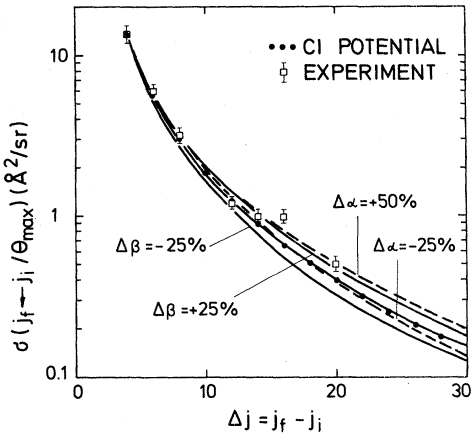

FIG. 15. Variation of the relative magnitude of the cross section at the rainbow maximum as the anisotropy and the steepness of the interaction potential are varied. The collision energy is 190 meV and $j_i=9$. Parameters $\Delta\beta$ and $\Delta\alpha$ are defined in Eqs. (18) and (19). Also shown are the results of the original *ab initio* interaction potential V_{CI} and the experimental data. All curves are normalized to the $j_i=9$ to $j_f=13$ rainbow intensity as obtained from V_{CI}.

leaving the interaction potential above 10 meV unchanged has also no noticeable effect on the calculated cross section for scattering angles larger than $\theta_{c.m.}=5°$. As is pointed out in Sec. III the calculation of the potential-energy surface has not been designed for a quantitative description of the region ot the van der Waals well. The error of the well depth is expected, however, to be significantly smaller than a factor of 2.

Finer details of the angular variation of the cross sections such as the phase and amplitude of supernumerary rainbow oscillations could be used in principle as an added check on the limits of accuracy of the *ab initio* potential surface. This has not been done because within the experimental error of the transformed data the sensitivity is not high enough as proved by calculating a few trial cross sections. In part this may also be attributed to the energy spread of the two colliding beams which tends to eliminate the finer details of the cross sections.

VIII. SUMMARY

We have reported the results of a systematic investigation, both experimentally and theoretically, of the state-to-state rotational energy and momentum transfer in the angularly resolved scattering of Na_2 from Ne. The variation of the shape and relative magnitude of differential cross sections with Δj at fixed j_i as well as j_i at fixed Δj has been investigated and interpreted. The present set of data represents one of the largest and most detailed sets of experimental state-to-state differential cross sections available for atom-diatom scattering from a steeply repulsive potential. Theoretical cross sections, calculated within the infinite-order sudden approximation using an *ab initio* potential surface, provided an excellent representation of the experimental data as was demonstrated by comparison in the center-of-mass reference frame. The extent to which this agreement could be used to place limits upon the accuracy of the *ab initio* surface was investigated through a systematic varying of the potential-energy surface. The results of this analysis point out the desirability of being able to extend the range of the experimentally measurable rotational transitions to larger values of Δj, *provided the angular resolution is maintained,* as well as the range of available collision energies. Efforts are currently underway in these directions.

ACKNOWLEDGMENTS

We gratefully acknowledge the support of the Deutsche Forschungsgemeinschaft through Sonderforschungsbereich 91 "Energietransfer bei atomaren und molekularen Stössen." We also thank E. Gottwald for help in the data analysis and H.-J. Korsch for many useful discussions. One of us, K. B., would also like to thank D. Krause (Schott/Mainz) and H. Karstensen (TU Braunschweig) for the development of the fibers necessary for the experiment. This work is based in part on the thesis of U. Hefter, submitted in partial requirement for the Ph.D. at the Universität Kaiserslautern.

[1]H. G. Bennewitz, K. H. Kramer, W. Paul, and J. P. Toennies, Z. Phys. 177, 84 (1964); J. P. Toennies, *ibid.* 182, 257 (1965).

[2]A. R. Blythe, A. E. Grosser, and R. B. Bernstein, J. Chem. Phys. 41, 1917 (1964).

[3]J. I. Steinfeld and W. Klemperer, J. Chem. Phys. 42, 3475 (1965); K. Bergmann and W. Demtröder, Z. Phys. 243, 1 (1971); K. Bergmann, W. Demtröder, M.

Stock, and G. Vogl, J. Phys. B 7, 2036 (1974); Ch. Ottinger and D. Poppe, Chem. Phys. Lett. 8, 513 (1971).
[4]J. C. Polanyi and K. B. Woodall, J. Chem. Phys. 56, 1563 (1972); J. A. Barnes, M. Keil, R. E. Kutina, and J. C. Polanyi, *ibid.* 72, 6306 (1980); 76, 913 (1982).
[5]Ch. Ottinger and M. Schröder, J. Phys. B 12, 3533 (1979).
[6]B. E. Wilcomb and P. J. Dagdigian, J. Chem. Phys. 67, 3829 (1977); P. J. Dagdigian, B. E. Wilcomb, and M. H. Alexander, *ibid.* 71, 1760 (1979); P. J. Dagdigian and B. E. Wilcomb, *ibid.* 72, 6462 (1980); U. Borkenhagen, H. Malthan, and J. P. Toennies, *ibid.* 71, 1722 (1979); G. Meyer and J. P. Toennies, *ibid.* 75, 2753 (1981).
[7]N. Smith, T. A. Brunner, A. W. Karp, and D. E. Pritchard, Phys. Rev. Lett. 43, 693 (1979); T. A. Brunner, R. D. Driver, N. Smith, and D. E. Pritchard, J. Chem. Phys. 70, 4155 (1979); N. Smith, A. Brunner, and D. E. Pritchard, *ibid.* 74, 467 (1981); T. A. Brunner, N. Smith, A. W. Karp, and D. E. Pritchard, *ibid.* 74, 3324 (1981).
[8]H. Schmidt, V. Hermann, and F. Linder, J. Chem. Phys. 69, 2734 (1978); W. Eastes, U. Ross, and J. P. Toennies, Chem. Phys. 39, 407 (1979); M. Faubel and J. P. Toennies, J. Chem. Phys. 71, 3770 (1979).
[9]U. Buck, F. Huisken, J. Schleusener, and H. Pauly, Phys. Rev. Lett. 38, 680 (1977).
[10]W. R. Gentry and C. F. Giese, J. Chem. Phys. 67, 6380 (1977); Phys. Rev. Lett. 39, 1259 (1977); U. Buck, F. Huisken, and J. Schleusener, J. Chem. Phys. 68, 5654 (1978); U. Buck, F. Huisken, J. Schleusener, and J. Schäefer, *ibid.* 74, 535 (1981).
[11]K. Bergmann, R. Engelhardt, U. Hefter, and J. Witt, Phys. Rev. Lett. 40, 1446 (1978).
[12]K. Bergmann, R. Engelhardt, U. Hefter, and J. Witt, J. Chem. Phys. 71, 2726 (1979).
[13]K. Bergmann, U. Hefter, and J. Witt, J. Chem. Phys. 72, 4777 (1980).
[14]K. Bergmann, U. Hefter, A. Mattheus, and J. Witt, Chem. Phys. Lett. 78, 61 (1981).
[15]U. Hefter, P. L. Jones, A. Mattheus, J. Witt, K. Bergmann, and R. Schinke, Phys. Rev. Lett. 46, 915 (1981).
[16]J. A. Serri, A. Morales, W. Moskowitz, D. E. Pritchard, C. H. Becker, and J. L. Kinsey, J. Chem. Phys. 72, 6304 (1980).
[17]J. A. Serri, C. H. Becker, M. B. Elbel, J. L. Kinsey, W. P. Moskowitz, and D. E. Pritchard, J. Chem. Phys. 74, 5116 (1981).
[18]W. Schepper, U. Ross, and D. Beck, Z. Phys. A 290, 131 (1979); D. Beck, U. Ross, and U. Schepper, Phys. Rev. A 19, 2173 (1979).
[19]M. Faubel, K.H. Kohl, and J. P. Toennies, J. Chem. Phys. 73, 2506 (1980).
[20](a) J. P. Toennies, Annu. Rev. Phys. Chem. 27, 225 (1976); (b) M. Faubel and J. P. Toennies, Adv. At. Mol. Phys. 13, 229 (1977).
[21]H. Loesch, Adv. Chem. Phys. 42, 421 (1980).
[22]H. Pauly, in *Atom-Molecule Collision Theory,* edited by R. B. Bernstein (Plenum, New York, 1979).
[23]R. B. Gerber, V. Buch, and U. Buck, J. Chem. Phys. 72, 3596 (1980); R. B. Gerber, V. Buch, U. Buck, G. Maneke, and J. Schleusener, Phys. Rev. Lett. 44, 1397 (1980); J. Andres, U. Buck, F. Huisken, J. Schleusener, and F. Torello, J. Chem. Phys. 73, 5620 (1980).
[24]D. Beck, U. Ross, and W. Schepper, Z. Phys. A 293, 107 (1979).
[25]D. Beck, U. Ross, and W. Schepper, Z. Phys. A 299, 97 (1981).
[26]L. D. Thomas, J. Chem. Phys. 67, 5224 (1977).
[27](a) S. Bosanac, Phys. Rev. A 22, 2617 (1980); (b) H. J. Korsch and D. Richards, J. Phys. B 14, 1973 (1981); (c) H. J. Korsch and D. Poppe, Chem. Phys. (in press).
[28]R. Schinke, Chem. Phys. 34, 65 (1978).
[29]J. M. Bowman, Chem. Phys. Lett. 62, 309 (1979).
[30]R. Schinke and P. McGuire, J. Chem. Phys. 71, 4201 (1979).
[31]R. Schinke, J. Chem. Phys. 72, 1120 (1980).
[32]R. Schinke, Chem. Phys. 47, 287 (1980); R. Schinke and H. J. Korsch, Chem. Phys. Lett. 74, 449 (1980).
[33]H. J. Korsch and R. Schinke, J. Chem. Phys. 73, 1222 (1980).
[34]R. Schinke and J. M. Bowman, in *Molecular Collision Dynamics,* edited by J. M. Bowman (Springer, Heidelberg, 1982).
[35]R. Schinke, J. Chem. Phys. 73, 6117 (1980).
[36]A collision energy of 175 meV has been quoted previously (see Ref. 14). This is slightly too low because the Na_2 beam velocity is 1415 ms^{-1} and not the 1350 ms^{-1} given.
[37]K. Bergmann, U. Hefter, and P. Hering, Chem. Phys. 32, 329 (1978); K. Bergmann, R. Engelhardt, U. Hefter, and P. Hering, *ibid.* 44, 23 (1979).
[38]K. Bergmann, R. Engelhardt, U. Hefter, and J. Witt, J. Phys. E 12, 507 (1979).
[39]J. Witt, Ph.D. thesis, University of Kaiserslautern, 1980 (unpublished).
[40]M. E. Kaminsky, J. Chem. Phys. 66, 4951 (1977).
[41]U. Hefter, Ph.D. thesis, University of Kaiserslautern, 1981 (unpublished).
[42]A. Mattheus, diplom-thesis, University of Kaiserslautern, 1981 (unpublished).
[43]W. Meyer, J. Chem. Phys. 64, 2901 (1976).
[44]R. Schinke, W. Müller, and W. Meyer, J. Chem. Phys. 76, 895 (1982).
[45]W. Demtröder and M. Stock, J. Mol. Spectrosc. 55, 476 (1975).
[46]W. Müller and R. Schinke, J. Chem. Phys. 75, 1219 (1981).
[47]R. Schinke, W. Müller, W. Meyer, and P. McGuire, J. Chem. Phys. 74, 3916 (1981).
[48]K. H. Kramer and R. B. Bernstein, J. Chem. Phys. 40, 200 (1964); C. F. Curtiss, *ibid.* 48, 1725 (1968) and 49, 1952 (1968); T. P. Tsien and R. T. Pack, *ibid.* 59, 5373 (1973); M. A. Brandt and D. G. Truhlar, Chem. Phys. Lett. 23, 48 (1973); D. Secrest, J. Chem. Phys. 72, 710

(1975).

[49]A. S. Dickinson, Comput. Phys. Commun. 17, 51 (1979).

[50]D. J. Kouri, in *Atom-Molecule Collision Theory,* edited by R. B. Bernstein (Plenum, New York, 1979).

[51]P. McGuire and D. J. Kouri, J. Chem. Phys. 60, 2488 (1974); R. T. Pack, *ibid.* 60, 603 (1974).

[52]K. W. Ford and J. A. Wheeler, Ann. Phys. (Paris) 7, 259 (1959).

[53]The Van der Waals minimum with a calculated average well depth of 0.3 meV causes a shallow minimum in the deflection function at large impact parameters. It has no consequences for the present calculation and affects only the region of extremely small scattering angles.

[54]W. H. Miller, Adv. Chem. Phys. 25, 69 (1974); 30, 77 (1975).

[55]The classification of rainbows into different types has been discussed by L. D. Thomas [J. Chem. Phys. 73, 5905 (1980)] and by J. M. Bowman and K. T. Lee [J. Chem. Phys. 74, 2664 (1981)]. See also Refs. 34 and 44.

[56]H. J. Korsch and R. Schinke, J. Chem. Phys. 75, 3850 (1981).

[57]S. I. Chu and A. Dalgarno, Proc. R. Soc. London, Ser. A: 342, 191 (1975); R. Goldflam, S. Green, and D. J. Kouri, J. Chem. Phys. 67, 4149 (1977); R. Goldflam, D. J. Kouri, and S. Green, *ibid.* 67, 5661 (1977); S. A. Parker and R. T. Pack, *ibid.* 68, 1585 (1978); R. Schinke and P. McGuire, Chem. Phys. 35, 391 (1978); S. S. Bhattacharyya and A. S. Dickinson, J. Phys. B 12, L521 (1979).

[58]V. Khare, J. Chem. Phys. 68, 4631 (1978).

[59]See, for example, M. Shapiro, R. B. Gerber, U. Buck, and J. Schleusener, J. Chem. Phys. 67, 3570 (1977) and Ref. 20 (b), p. 257 ff.

[60]W. Langbein and A. Mattheus, Comput. Phys. Commun. 21, 279 (1981).

[61]The transformed results presented in Fig. 3 of Ref. 14 are slightly in error in the backward direction. The assumed collision energy was approximately 8% too low (see Ref. 36). This affects the predicted angular position of the kinematic peak in the laboratory frame. The apparent shoulder in the center-of-mass cross sections at large scattering angles results from the improper deconvolution of this peak.

[62]T. A. Brunner, N. Smith, A. W. Karp, and D. E. Pritchard, J. Chem. Phys. 74, 3324 (1981).

[63]J. C. Polanyi and K. B. Woodall, J. Chem. Phys. 56, 1563 (1972); R. D. Levine, R. B. Bernstein, P. Kahana, I. Procaccia, and E. T. Upchurch, *ibid.* 64, 796 (1976); I. Procaccia and R. D. Levine, *ibid.* 64, 808 (1976).

[64]A. E. DePristo, S. D. Augustin, R. Ramaswany, and H. Rabitz, J. Chem. Phys. 75, 850 (1979).

[65]R. Schinke, J. Chem. Phys. 75, 5205 (1981); 75, 5449 (1981).

[66]E. F. Jendrek and M. H. Alexander, J. Chem. Phys. 72, 6452 (1980).

[67]I. N. Batcha and N. Sathyamurthy, Chem. Phys. Lett. 79, 264 (1981).

[68]U. Buck, F. Huisken, J. Schleusener, and J. Schäfer, J. Chem. Phys. 72, 1512 (1980).